高压物理学报
CHINESE JOURNAL OF HIGH PRESSURE PHYSICS

第 32 卷 第 2 期
2018 年 4 月

高 压 物 理 学 报
CHINESE JOURNAL OF HIGH PRESSURE PHYSICS

Vol. 32, No. 2
Apr., 2018

DOI: 10.11858/gywlxb.20170571

Electrical Transport Properties of Hexagonal $TaSi_2$ Crystals Based on Structural Stability under High Pressure*

LI Xiaoyang, LU Yang, YAN Hao

(*Center for High Pressure Science and Technology Advanced Research, Shanghai* 201203, *China*)

Abstract: As a class of stable low-resistivity and high-temperature materials, tantalum disilicide ($TaSi_2$) has been widely used in integrated circuits. Therefore, its electrical stability is as important as its structural stability. Here, we report the electronic transport properties of $TaSi_2$ based on structural stability under high pressure. Its stable crystallographic structure was studied by synchrotron X-ray diffraction and Raman spectroscopy experiments up to 20 GPa. *In situ* high-pressure resistance measurements revealed that the resistivity of $TaSi_2$ has a trend to be steady at the value of about 2 $\mu\Omega \cdot$ cm under pressure increasing up to 16.3 GPa. Futher, the electronic structure of $TaSi_2$ under pressure was theoretically calculated to understand its metallic behavior.

Keywords: $TaSi_2$; high pressure; crystal structure; electrical transport properties

CLC number: O521.21 **Document code**: A

As a class of silicide compounds, metal silicides, such as $TaSi_2$, $TiSi_2$, WSi_2, Mg_2Si, $CrSi_2$ and Ta_5Si_3, have been extensively investigated due to their low resistivity, superior thermal stability and excellent oxidation resistance[1-4]. These silicides have been employed as coating materials for energy and aerospace[5-6], low resistance contacts and interconnects in large scale integrated circuits[7], gate materials for CMOS microelectronic devices[8], strain-sensitive materials for strain gauges[5] and thermoelectric materials for stable transducers[9]. Generally, the structural stability and electrical transport properties of materials are more attractive for the semiconductor industry, materials science and physics. In addition to temperature, pressure is an alternative approach to studying structural stability and physicochemical properties of materials, as well as to synthesizing new compounds and exploring novel physical mechanisms[10]. Recently, Li *et al*.[11] found that the hexagonal C40 structure of $TaSi_2$ is stable in a wide pressure range (0−50 GPa). Electronic devices made of metal silicides, like $TaSi_2$, may become available under stress or pressure if electrical transport properties permit.

The intrinsic electrical properties of metal silicides have long been studied at different temperatures. For $TaSi_2$, superconductivity has been found below the critical temperatures of 0.35 and 4.4 K for bulk single crystals and a thin-film on sapphire as substrate, respectively[12-13]. The electrical resistivity of the $TaSi_2$ single crystal along the $\langle 0001 \rangle$ crystallographic direction was less than along the $\langle 10\bar{1}0 \rangle$ direction in the range of 4.2−1100 K and the anisotropy of electrical resistivity at room temperature was almost 100%[14]. The current-voltage characteristics of the $TaSi_2$/n-Si junction were also investi-

* **Received date**: 2017-04-26; **Revised date**: 2017-05-03
Foundation Item: National Natural Science Foundation of China(U1530402)
Biography: LI Xiaoyang(1991—), male, master, major in condensed matter physics. E-mail: xiaoyang.li@hpstar.ac.cn
Corresponding author: YAN Hao(1975—), male, doctor, major in condensed matter physics. E-mail: yanhao@hpstar.ac.cn

gated at different temperatures and the junction exhibited Schottky behavior[15]. However, the electrical transport properties of metal silicides under high pressure have rarely been reported.

In this work, we used $TaSi_2$ as an example metal silicide to study electrical stability at high pressure and room temperature. The structural stability of $TaSi_2$ powder was examined by *in situ* synchrotron X-ray diffraction (XRD) and Raman spectroscopy under pressures up to 20 GPa. The electrical stability is reflected by the electrical resistances of the sample under different pressures, which were measured using an *in situ* high-pressure four-probe method. Finally, the electronic energy band structure of $TaSi_2$ at 0 GPa and high pressure was calculated to explain the experimental results.

1 Experimental Section

1.1 *In situ* High-Pressure Characterizations

A Mao-Bell type symmetric diamond anvil cell (DAC) with 400 μm-diameter anvil culets was used to generate pressure. T301 stainless steel with a thickness of 250 μm was pre-indented to a thickness of ~50 μm to serve as gaskets. A 150 μm diameter hole was laser drilled (λ=1 064 nm) at the center of the pre-indentation to serve as the sample chamber. Then, $TaSi_2$ powder (Alfa Aesar, 99.9%) was loaded into the chamber, and silicone oil was used as a pressure-transmitting medium. A ruby ball preplaced at the center of the culet was employed to determine the pressure by the ruby fluorescence method[16].

The *in situ* high-pressure angle-dispersive X-ray diffraction (AD-XRD) experiments were performed at the BL15U1 beamline of the Shanghai Synchrotron Radiation Facility (SSRF) using a wavelength of 0.061 99 nm. The sample to detector distance was 170.5 mm. The obtained two-dimensional image data were converted to one-dimensional XRD patterns by Fit2D-WAXD software[17]. Rietveld refinements were conducted using the General Structure Analysis System (GSAS) with the user interface EXPGUI package[18-19]. The *in situ* high-pressure Raman scattering spectra were collected by a Raman spectrometer with an excitation laser (λ=532 nm, Renishaw 1000).

1.2 *In situ* High-Pressure Resistance Measurements

The pressure-dependent electrical resistance was measured using a four-probe method in a symmetric DAC with 500 μm-culet sized anvils. To create an insulated environment, a ~500 μm diameter hole was drilled in the pre-indented gasket, then the wall of the hole and indentation were fully coated with c-BN and the other gasket surface was covered with epoxy (AB gel). After that, four platinum electrodes (25 μm in thickness) were arranged on one side of the gasket to connect the copper leads and the sample in the chamber. There was no pressure transmitting medium inside the chamber. The resistance measurements were carried out on the as-fabricated microcircuit using electronic equipments (Keithley 6221 current source, 2182A nanovoltmeter, and 7001 switch system), and the pressure was determined by the ruby fluorescence. The resistivity was calculated according to the Van der Pauw method[20].

1.3 Theoretical Calculations of the Band Structure

The first-principle calculations of the electronic structure for hexagonal $TaSi_2$ under pressures of 0 and 15 GPa were performed using the CASTEP code[21] in the Materials Studio package with the geometry optimization. The convergence tolerance in the geometry optimization was 2.0×10^{-5} eV/atom. The optimization was completed when the forces were less than 0.5 eV/nm and all stress components were less than 0.1 GPa. At each pressure, a generalized gradient approximation of the Perdew-Burke-Ernzerhof (GGA-PBE) version functional of the exchange-correlation was adopted to optimize the lattice parameters for hexagonal C40 which takes the actual situation such as electron correlations into consideration.

2　Results and Discussion

2.1　Structural Stability

Here, we studied a hexagonal structure of $TaSi_2$ sample. The X-ray diffraction patterns of the sample under compression and decompression are shown in Fig. 1(b). Upon compression to 20.1 GPa all the Bragg peaks shifted towards high angles, revealing the shrinkage of the $TaSi_2$ unit cell. There was no significant variation in the XRD patterns in the number and shape of the diffraction peaks. The Bragg peaks reverted to their previous positions after decompression to ambient pressure. Fig. 1(c) shows a typical GSAS refinement of the XRD pattern at 1.0 GPa. The detailed crystallographic information for low and high-pressure phases of $TaSi_2$ was shown in Table 1.

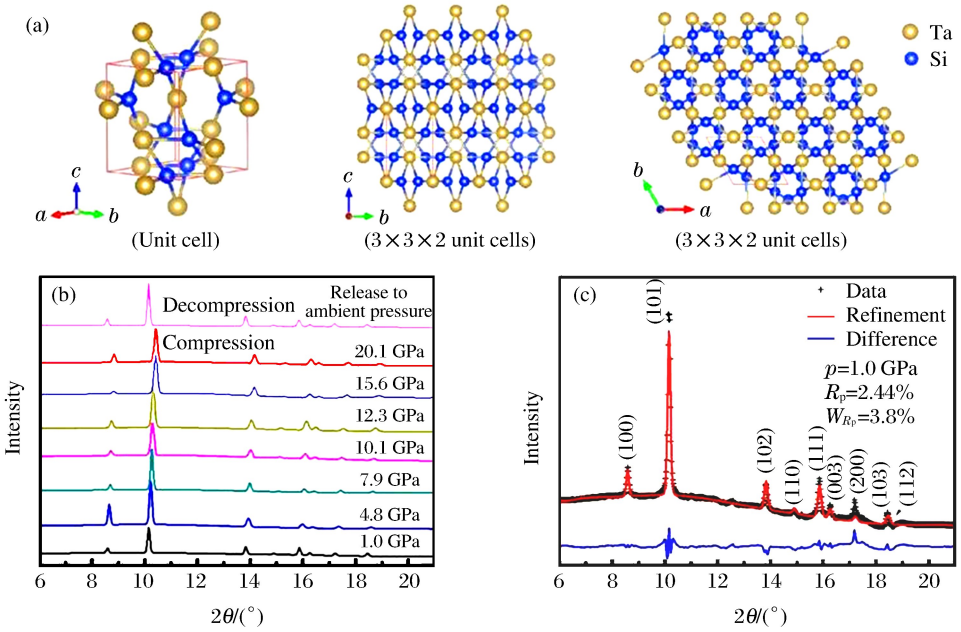

Fig. 1　(a) Crystal structure of $TaSi_2$ in ambient conditions; (b) Synchrotron XRD patterns of $TaSi_2$ during compression and decompression; (c) Refinement of $TaSi_2$ XRD data at 1.0 GPa

Table 1　Rietveld refinement results of $TaSi_2$ under low pressure and high pressure

Pressure/GPa	Atom type	Fractional coordinates
1	Ta	(0.5, 0, 0)
1	Si	(0.16 148 66, 0.32 296 3, 0)
20	Ta	(0.5, 0.32 296 30, 0)
20	Si	(0.17 069 90, 0.34 138 9, 0)

The good refinements confirm that the hexagonal structure of $TaSi_2$ is very stable without phase transitions during compression up to 20 GPa and decompression to ambient conditions. These results are consistent with a previous study[11]. From the refinements of all the diffraction patterns, the compressive behavior of the $TaSi_2$ lattice cell can be obtained. Fig. 2(a) shows the pressure dependence of the $TaSi_2$ lattice parameters and volume. We found that the a and c lattice parameters and the unit cell volume V decreased with increasing pressure. The normalized lattice parameters as a function of pressure shown in Fig. 2(b) reveal that the a axis was more compressible than the c axis and anisotropic compression increased with increasing pressure. This anisotropy of $TaSi_2$ under compression can be

attributed to the relatively compact stacking along the 〈0001〉 direction[11] (Fig. 1(a)). Through third-order Birch-Murnaghan equation of state (EOS) fitting we can get the bulk modulus of hexagonal phase of $TaSi_2$ as 203(2) GPa, as shown in Fig. 2(c). In addition, the bulk modulus of $TaSi_2$ is too big to be easily compressed.

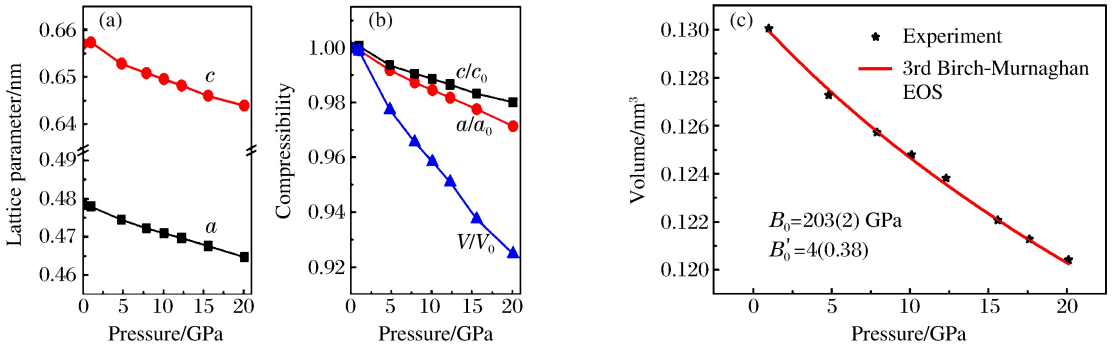

Fig. 2　(a) Pressure-dependent lattice parameters of $TaSi_2$ (a_0 = 0.478 4 nm, c_0 = 0.657 0 nm); (b) Evolution of the normalized lattice parameters and volume with pressure for $TaSi_2$; (c) Pressure-dependent unit cell volume of $TaSi_2$

Highly sensitive Raman spectroscopy was employed to obtain local structure information. Fig. 3(a) shows the Raman spectra of the sample collected during pressurization from ambient to high pressure and release to ambient pressure. From the Raman spectrum at ambient pressure, four Raman peaks can be observed at the centered frequencies of 145.0, 290.0, 355.0 and 503.8 cm^{-1}, denoted as A_1, A_2, A_3 and A_4, respectively. The peak A_4 could be related to the Si—Si vibration mode. During the compression-decompression cycle, these Raman modes can almost be clearly observed. Upon decompression to ambient pressure, the Raman modes A_1, A_2 and A_3 were found to revert to their original frequencies, but the Si—Si vibration mode A_4 was hysteretic. The vibrational frequencies of two obvious Raman peaks (A_3 and A_4) as a function of pressure are shown in Fig. 3(b) and exhibit blue shift under compression due to the shortening of the Si—Ta—Si and Si—Si bond. These findings indicate the local structural stability of the $TaSi_2$ particles under pressure, which corresponds to the structural stability analysis from XRD results.

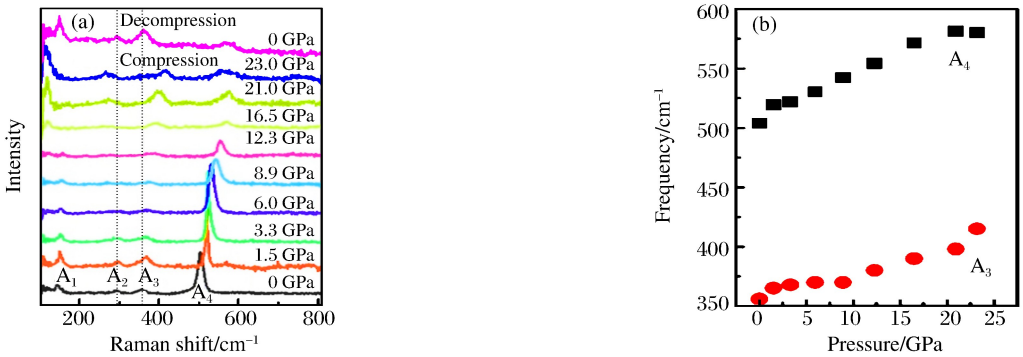

Fig. 3　(a) Pressure-dependent Raman spectra of $TaSi_2$ at room temperature; (b) Pressure-dependent Raman peaks (A_3 and A_4) of $TaSi_2$ derived from the Raman spectra

2.2　Electrical Stability

In general, decreasing the distance between the atoms and the interlayers of a crystal material under external pressure or stress can alter its electronic behavior[22]. Sometimes, this effect may adversely affect

the stability of electronic devices under stress. Here, the electronic transport properties of $TaSi_2$ under different pressures are expressed by the electrical resistance, which was measured by a four-probe method using a fabricated microcircuit in a DAC (Fig. 4 inset). As shown in Fig. 4, the electrical resistance of the sample decreased dramatically with pressure increasing up to 5 GPa due to the gradually closer contact between the $TaSi_2$ particles. In the high-pressure region (5.0−16.3 GPa), the resistance trend was steady with increasing pressure and the resistance reduced by less than half. The resistance during decompression and compression was almost consistent in the high-pressure region. Therefore, the electrical transport properties of $TaSi_2$ are very stable in the high-pressure region during compression and decompression.

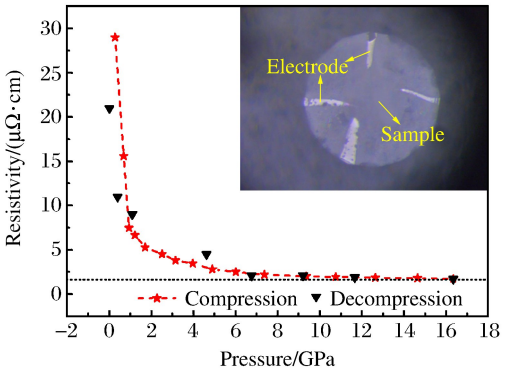

Fig. 4　The resistivity of $TaSi_2$ under pressure at room temperature (The inset (upper right) is a photograph of the four-probe microcircuit in the diamond anvil cell.)

A previous study reported that the resistivity of a $TaSi_2$ single crystal at ambient pressure and temperature was approximately 20 μΩ·cm along the 〈0001〉 crystallographic direction and 40 μΩ·cm along the $\langle 10\bar{1}0\rangle$ direction[23]. Hence, $TaSi_2$ exhibits metallic behavior. In our case, the pressure-dependent resistivity of the sample consisted of many particles, as shown in the Fig. 4 inset. Thus, the resistivity under pressures of 5.0 and 16.3 GPa was about 2.8 and 1.7 μΩ·cm, respectively. That is to say, the resistivity of $TaSi_2$ decreased by one order of magnitude at room temperature from ambient pressure to 5.0 GPa. The metallicity of $TaSi_2$ obviously increased with the increase of applied pressure. Therefore, it is conceivable that electronic devices made of $TaSi_2$ may work well under pressure and release less waste heat.

To further understand $TaSi_2$ electrical stability and illuminate the underlying physical mechanism of its resistivity-pressure relationship, its band structures under ambient pressure and high pressure were calculated by first-principle calculations. Fig. 5 shows the electronic band structure of $TaSi_2$ at ambient pressure and 15 GPa. Their topological geometries are considerably similar, *i.e.*, the electronic energy band structure is very stable under high pressure. The difference is that the electronic energy band broadens under high pressure compared to that under ambient pressure, which is due to shorten-

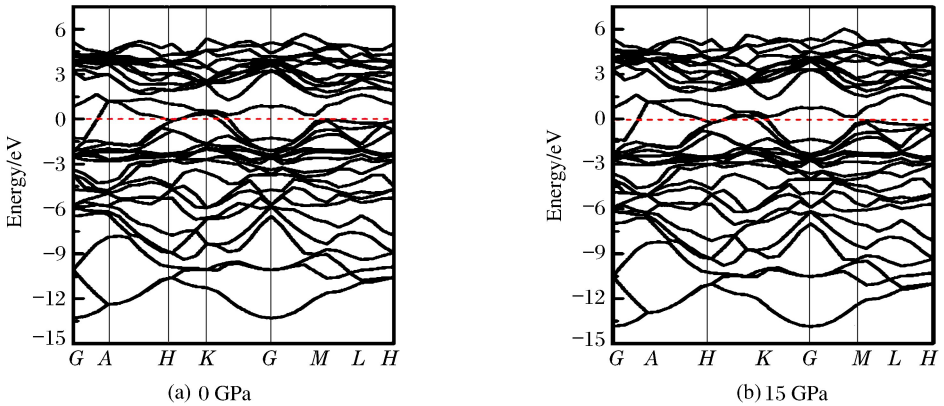

Fig. 5　Calculated band structure of $TaSi_2$ at (a) 0 GPa and (b) 15 GPa

ing of the lattice parameters. Moreover, the Fermi surface of $TaSi_2$ under ambient pressure and 15 GPa locates below the top of the valence band and the valence-band maximum crosses the conduction-band minimum, *i. e.*, the band gap disappears. This demonstrates that $TaSi_2$ shows metallic behavior, which can contribute to the low-resistivity of $TaSi_2$ under ambient and high pressure.

3 Conclusions

In summary, we studied the crystallographic structural stability and electrical transport properties of metallic $TaSi_2$ under high pressure using angle-dispersive synchrotron XRD, Raman spectroscopy, and four-probe resistance measurements as well as first-principle calculations. The *in situ* high-pressure XRD and Raman characterizations demonstrated that the structure was stable up to 20 GPa, consistent with a previously reported result. The resistivity of $TaSi_2$ was steady at $\sim 2\ \mu\Omega \cdot$ cm under pressures from ambient pressure to 16.3 GPa. First-principle calculations showed that the topological geometries of the $TaSi_2$ electronic structure under ambient and high pressure were similar and their valence-band maximums were located over the Fermi surface, which was responsible for its electrical stability and metallic behavior.

References:

[1] SUBRAHMANYAM J, RAO R M. Combustion synthesis of $MoSi_2$, WSi_2 alloys [J]. Materials Science & Engineering A, 1994, 183(1/2): 205-210.

[2] ITO K, YANO T, NAKAMOTO T, et al. Microstructure and mechanical properties of $MoSi_2$ single crystals and directionally solidified $MoSi_2$-based alloys [J]. Progress in Materials Science, 1997, 42(1/2/3/4): 193-207.

[3] ITO K, NAKAMOTO T, INUI H, et al. Stacking faults on (001) in transition-metal disilicides with the cllb structure [C]//MRS Proceedings. Cambridge: Cambridge University Press, 1996, 460: 599.

[4] HAO J, ZOU B, ZHU P W, et al. *In situ* X-ray observation of phase transitions in MgSi under high pressure [J]. Solid State Communications, 2009, 149(17): 689-692.

[5] SCHULTES G, SCHMITT M, GOETTEL D, et al. Strain sensitivity of TiB_2, $TiSi_2$, $TaSi_2$ and WSi_2 thin films as possible candidates for high temperature strain gauges [J]. Sensors & Actuators A: Physical, 2006, 126(2): 287-291.

[6] SCHMITT A L, HIGGINS J M, SZCZECH J R, et al. Synthesis and applications of metal silicide nanowires [J]. Journal of Materials Chemistry, 2009, 20(2): 223-235.

[7] JIANG D E, CARTER E A. First-principles study of the interfacial adhesion between SiO_2 and $MoSi_2$ [J]. Physical Review B, 2005, 72(16): 165410.

[8] LAVOIE C, D'HEURLE F M, DETAVERNIER C, et al. Towards implementation of a nickel silicide process for CMOS technologies [J]. Microelectronic Engineering, 2003, 70(2/3/4): 144-157.

[9] NAGASE T, YAMAUCHI I, OHNAKA I. Effect of rapid solidification on microstructure of various $Fe_{29.5-x}Si_{70.5-x}$ ($0.0 \leqslant x \leqslant 3.7$) alloys [J]. Journal of Alloys & Compounds, 2000, 312(1): 295-301.

[10] ZHANG S L, ÖSTLING M. Metal silicides in CMOS technology: past, present, and future trends [J]. Critical Reviews in Solid State & Materials Sciences, 2003, 28(1): 1-129.

[11] LI C Y, YU Z H, LIU H Z, et al. High pressure and high temperature *in situ* X-ray diffraction study on the structural stability of tantalum disilicide [J]. Solid State Communications, 2013, 157: 1-5.

[12] KNOEDLER C M, DOUGLASS D H. Superconductivity in $NbGe_2$, and isostructural C-40 compounds [J]. Journal of Low Temperature Physics, 1979, 37(1/2): 189-218.

[13] GOTTLIEB U, LASJAUNIAS J C, THOLENCE J L, et al. Superconductivity in $TaSi_2$ single crystals [J]. Physical

Review B, 1992, 45(9): 4803-4806.

[14] NAVA F, MAZZEGA E, MICHELINI M, et al. Analysis of the electrical resistivity of Ti, Mo, Ta, and W monocrystalline disilicides [J]. Journal of Applied Physics, 1989, 65(4): 1584-1590.

[15] ABU-SAMAHA F S, DARWISH A A A, MANSOUR A N. Temperature dependent of the current-voltage (*I-V*) characteristics of $TaSi_2$/n-Si structure [J]. Materials Science in Semiconductor Processing, 2013, 16(6): 1988-1991.

[16] MAO H K, XU J A, BELL P M. Calibration of the ruby pressure gauge to 800 kbar under quasi-hydrostatic conditions [J]. Journal of Geophysical Research: Solid Earth, 1986, 91(B5): 4673-4676.

[17] HAMMERSLEY A P, SVENSSON S O, HANFLAND M, et al. Two-dimensional detector software: from real detector to idealised image or two-theta scan [J]. High Pressure Research, 1996, 14(4/5/6): 14.

[18] LARSON A C, VON DREELE R B. General structure analysis system (GSAS): LAUR 86-748 [R]. USA: Los Alamos National Laboratory, 2004.

[19] TOBY B H. EXPGUI, a graphical user interface for GSAS [J]. Journal of Applied Crystallography, 2001, 34(2): 210-213.

[20] RAMADAN A A, GOULD R D, ASHOUR A. On the Van der Pauw method of resistivity measurements [J]. Thin Solid Films, 1994, 239(2): 272-275.

[21] SEGALL M D, LINDAN P J D, PROBERT M J, et al. First-principles simulation: ideas, illustrations and the CASTEP code [J]. Journal of Physics: Condensed Matter, 2002, 14(11): 2717-2744.

[22] KOSOBUTSKY A V, SARKISOV S Y, BRUDNYI V N. Structural, elastic and electronic properties of GaSe under biaxial and uniaxial compressive stress [J]. Journal of Physics & Chemistry of Solids, 2013, 74(9): 1240-1248.

[23] NAVA F, MAZZEGA E, MICHELINI M, et al. Analysis of the electrical resistivity of Ti, Mo, Ta, and W monocrystalline disilicides [J]. Journal of Applied Physics, 1989, 65(4): 1584-1590.

高压下六方 $TaSi_2$ 晶体基于结构稳定性的电学输运性质

李晓阳，陆　阳，晏　浩

（北京高压科学研究中心，上海　201203）

摘要：作为一类稳定的低电阻及高温材料，二硅化钽（$TaSi_2$）被广泛应用于集成电路中。因此，其电学稳定性和结构稳定性同样重要。报导了高压下六方 $TaSi_2$ 晶体基于结构稳定性的电学输运性质。通过同步辐射 X 射线衍射和拉曼光谱实验研究了 $TaSi_2$ 晶体在压力高达 20 GPa 时稳定的结晶学结构，并通过原位高压电阻测量发现，当压力增加到 16.3 GPa 时，$TaSi_2$ 的电阻率趋于稳定在 2 μΩ·cm 左右；进一步理论计算了压力下 $TaSi_2$ 的电子结构，以进一步理解其金属性行为。

关键词：二硅化钽；高压；晶体结构；电学输运性质

中图分类号：O521.21　　**文献标志码**：A